Available online at www.sciencedirect.com

ScienceDirect

Procedia Engineering 203 (2017) 336–348

Procedia Engineering

www.elsevier.com/locate/procedia

26th International Meshing Roundtable, IMR26, 18-21 September 2017, Barcelona, Spain

Generalized Regular Quadrilateral Mesh Generation based on Surface Foliation

Na Lei[a,d,e], Xiaopeng Zheng[a,d,*], Hang Si[b], Zhongxuan Luo[a,d], Xianfeng Gu[c,e]

[a]*DUT-RU International School of Information Science and Engineering, Dalian University of Technology, Dalian 116620, China*
[b]*Weierstrass Institute for Applied Analysis and Stochastics, Berlin 10117, Germany*
[c]*Computer Science Department, Stony Brook University, Stony Brook 11794 NY, USA*
[d]*Key Laboratory for Ubiquitous Network and Service Software of Liaoning Province, Dalian 116620, China*
[e]*Beijing Advanced Innovation Center for Imaging Technology, Capital Normal University, Beijing 100048, China*

Abstract

This work introduces a novel algorithm for quad-mesh generation based on surface foliation theory. The algorithm is based on the equivalence among colorable quad-meshes, measure foliations and holomorphic differentials. The holomorphic differentials can be obtained by graph-valued harmonic maps. The algorithm has several merits: it can be applied for surfaces with general topologies; the resulting quad-meshes have global tensor product structure and the least number of singularities; the algorithmic pipeline is fully automatic. The experimental results demonstrate the efficiency and efficacy of the proposed method.

Peer-review under responsibility of the scientific committee of the 26th International Meshing Roundtable.

Keywords: quadrilateral; quad-mesh; structured; foliation; harmonic map; holomorphic differential;

1. Introduction

Polygonal meshes are ubiquitous in many engineering and medicine fields, such as computer graphics, computer vision, geometric modeling, mechanical engineering, architecture and medical imaging. Although triangle meshes are the most popular representations, quadrilateral meshes have many advantages and have been widely used CAD and simulation. The main advantages of quad-meshes can be summarized as follows:

- Quad-mesh can better capture the local principle curvature directions or sharp features, as well as the semantics of modeled objects, therefore it is widely used in animation industry.
- Quad-mesh has tensor product structure, it is suitable for fitting splines or NURBS. Therefore it is applied for high-order surface modeling, such as CAD/CAM for Splines and NURBS, and the entertainment industry for subdivision surfaces.
- Patches of semi-regular quad meshes with a rectangular grid topology, naturally match the sampling pattern of textures. Therefore quad-mesh is highly preferred for texturing and compression.

* Corresponding author. Tel.: +86-180-1047-2087.
E-mail address: shawnxpzheng@gmail.com

1877-7058
Peer-review under responsibility of the scientific committee of the 26th International Meshing Roundtable.
10.1016/j.proeng.2017.09.818

Given a quad-mesh, a vertex is called *regular*, if its topological valence is 4; otherwise, it is *singular*. A path consisting of a sequence of adjacent edges $\{e_0, e_1, \cdots, e_k\}$ is called a *separatrice*, if it starts from and ends at singularities, and each pair of consecutive edges e_i, e_{i+1} share the same regular vertex v_i, furthermore e_i and e_{i+1} belong to different faces. The regularity of the quad-mesh can be described by the number of singularities, and the global behavior of the separatrices.

Roughly speaking, quad-meshes can be classified to four categories with the descending regularity:

1. Regular quad-mesh: all the interior vertices are with topological valence 4, there are no singularities, such as geometry image [10]. The regular quad-mesh has strong topological restriction, we can never construct regular quad-mesh on the high genus $g > 1$ surface.
2. Semi-regular quad-mesh: The separatrices divide the quad-mesh into several topological rectangles (a topological disk with four corners on the boundary), the interior of each topological rectangle is regular grids.
3. Valence semi-regular quad-mesh: The number of singularities are few, but the separatrices have complicated global behavior, they may have intersections, form spirals and go through most edges.
4. Unstructured quad-mesh: if a large fraction of its vertices are irregular. For example, one can convert a triangle mesh to an unstructured quad-mesh by splitting each triangle into three quads by connecting the edge center to the face center.

1.1. Generalized Regular Quad-Mesh

The current work focuses on a special class of quad-meshes, which is between regular and semi-regular categories, which we call *generalized regular quad-mesh*. The generalized regular quad-mesh has only the valence 6 singular vertices and the number of the singular vertices reaches the theoretic lower bound. The theoretic lower bound of the number of the valence 6 singular vertices for a genus $g > 1$ close surface is $4g - 4$. A generalized regular quad-mesh combines the advantages of both regular and semi-regular quad-meshes, and overcome their disadvantages. Comparing to regular quad-meshes, generalized regular quad-meshes have no topological restrictions; comparing to semi-regular quad-meshes, generalized regular quad-meshes have more regular global structures, which consist of topological cylinders and reduce the number of singularities to the theoretic lower bound.

Our method is based on the following observations: by subdividing a generalized regular quad-mesh infinitely many times, one obtain two conjugate foliations; the foliations are equivalent to holomorphic quadratic differentials; a holomorphic quadratic differential can be obtained by a graph-valued harmonic mapping. Therefore, one can construct a pants decomposition of the surface, then convert the pants decomposition to a graph, compute the harmonic mapping from the surface to the graph, induce the conjugate foliations from the harmonic mapping, produce the generalized regular quad-mesh from the foliations, as shown in Fig. 4 and Fig. 9.

1.2. Previous Works

The literature of quad-meshing is huge, in the following we only review the most relevant works. We refer readers to [3] for a thorough literature review.

Triangle Mesh to Quad-Mesh Conversion. This method directly converts a triangle mesh to a quad-mesh. One naive way is to perform topological Catmull-Clark subdivision [5] and the other way is to fuse two original adjacent triangles into one quad [12,23,24,27]. The quad shape is strongly dependent on the input and the major drawback of this approach is that the resulting meshes are unstructured quad-meshes.

Patch Based Approach. This approach divides the input surface into several square patches, then by subdividing the patches to produce quad-meshes. This method can produce semi-regular quad-meshes. The singularities of the resulting quad-mesh arise where three, five or more patches meet. Clustering method (normal-based, center-based) [2,4] and poly-cube map [13,21,28,30] are adopted to compute the patches. Comparing to this approach, our algorithm produce much less number of singularities, the number is solely determined by the topology of the surface.

Parameterization Based Approach . There are many method in this category. The spectral surface quadrangulation method [7,14] derives the coarse quadrangular structure from the Morse-Smale complex of an eigenfunction of the Laplacian operator on the input mesh. Discrete harmonic forms [26], periodic Global Parameterization [1] and Branched Coverings method [17] are all use for quad mesh generation.

Most methods in this category can not produce semi-regular quad-meshes, but valence semi-regular ones. Namely, the global behavior of the separatrices are hard to control, which make the global structure intricate and reduce the regularity. In contrast, our method produce much higher regularity, the global behavior of separatrices is very simple. The surface is segmented by the separatrices (critical trajectories) into $3g-3$ topological cylinders.

Directional field Based Method. The paper [22] presented a novel method to approximate a surface with a planar quadrilateral mesh which was based on the study of conjugate direction fields. Starting with a triangle mesh, the method first compute an as smooth as possible conjugate direction field satisfying the users directional and angular constraints, then apply mixed-integer quadrangulation and planarization techniques to generate a planar quadrilateral mesh. The method can produce semi-regular quad mesh or valence semi-regular quad mesh. However it could neither control the mesh type directly, nor reduce the number of singularities to the lower bound. Compared to this methods, the quad meshes produced by our method have very clear and simple structures. Our algorithm produces one foliation and then the conjugate foliation, these two foliations form the quad mesh. For the quad mesh of a genus $g > 1$ close surface, all the interior singularities are all of valence 6 and their amount reaches the theoretic lower bound $4g-4$. The separatrices can divide the surface into $3g-3$ topological cylinders.

Voronoi Based Method. The paper [18] generates quad mesh by introducing Lp -Centroidal Voronoi Tessellation (Lp -CVT) and a generalization of CVT that allows for aligning the axes of the Voronoi cells with a predefined background tensor field. This method can only produce non-structured quad-mesh, there is no global tensor product structure.

1.3. Contributions

This work proposes a novel algorithm for quadrilateral meshing, the major contributions can be summarized as:

1. Discover a new category of quad-mesh - generalized regular quad-mesh, compared to regular quad-mesh, it can be applied for surfaces with general topologies; compared to semi-regular quad-mesh, it has higher regularity.
2. The generalized regular quad-mesh reduces the number of singularities to the theoretic lower bound (for a genus $g > 1$ closed surface, there are $4g-4$ singularities generically), and simplifies the global behavior of separatrices, (the separatrices divides the surface into $3g-3$ topological cylinders).
3. The generalized regular quad-mesh are with C^{∞} smoothness except the singular vertices and global tensor product structure, which are suitable for spline fitting application.
4. The algorithm has solid theoretic foundation, and is capable of constructing all structured quad-meshes based on surface foliation theory. There are infinite many such quad-meshes, all of them form a $6g-6$ linear space.
5. The algorithm can be fully automatic without any user input or intervention.

In the following discussion, we call generalized regular quad-mesh as regular quad-mesh, for the purpose of convenience.

2. Theoretic Foundation

Our proposed method is based on fundamental concepts and theorems in conformal geometry. Here we briefly review the basic concepts. Detailed treatments can be found in [8,11,15,25]. Additional concepts and theorems can be found in our previous work on hexahedral meshing based on surface foliation [19].

2.1. Overview

Our method is based on the equivalence among four key concepts: regular quad-mesh, colorable quad-mesh, Strebel differentials and graph-valued harmonic map. In this section, we give the solid theorems in topology and differential geometry.

Fig. 1: Equivalence among the key concepts.

1. Quad-meshes with minimal number of singularities are equivalent to colorable quad-meshes, explained in subsection 2.2;
2. Colorable quad-meshes are equivalent to measured foliations, detailed in subsection 2.2 and 2.3;
3. Measured foliations are equivalent to Strebel differentials, elucidated in subsection 2.4;
4. Strebel differentials are equivalent to graph-valued harmonic maps, illustrated in subsection 2.5.

These theorems lead to the practical computational algorithm for regular quad-meshes;

1. Construct a pants decomposition graph, find the harmonic map from the surface to the graph;
2. From the harmonic map to obtain the Strebel differential;
3. From the Strebel differential to get the foliations;
4. From the foliations to compute the regular quad-meshes.

2.2. Colorable Quadrilateral Mesh

Suppose S is a surface, a *quadrilateral mesh* of S is a geometric *cell decomposition*, such that each cell is topological quadrilateral. A vertex in a quadrilateral mesh is called *regular*, if its topological valence equals to 4; otherwise, the vertex is *irregular*. Irregular vertices are also called *singularities*. One of the major goal for quad-meshing is to minimize the number of irregular vertices.

A generic quad-mesh is called *regular*, if it is with the minimal number of singularities. We show that a quad-mesh is regular if and only if it is *colorable*.

Definition 1 (Colorable Quad Mesh). *Suppose Q is a quadrilateral mesh on a surface S, if there is a coloring scheme $\iota : E \to \{red, blue\}$, which colors each edge either red or blue, such that each quadrilateral face includes two opposite red edges and two opposite blue edges, then Q is called a colorable (red-blue) quadrilateral mesh.*

We show that the singularities of a colorable mesh are with even number of valences in [19].

Lemma 1. *Suppose S is an oriented closed surface, Q is a quadrilateral mesh on S. Q is colorable if and only if the valences of all vertices are even.*

2.3. Finite Measured Foliation

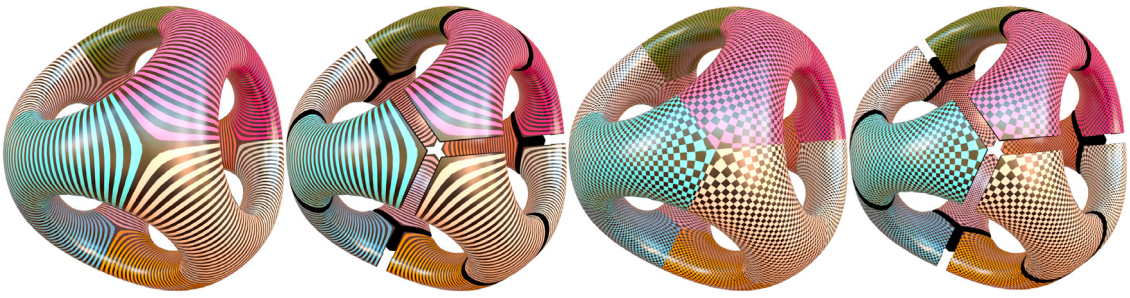

Fig. 2: Two conjugate finite measured foliations on a genus five surface.

Definition 2 (Measured Foliation). *Let S be a compact Riemann surface of genus $g > 1$. A C^k measured foliation on S with singularities $z_1, \ldots, z_l$ of order $k_1, \ldots, k_l$ respectively is given by an open covering $\{U_i\}$ of $S - \{z_1, \ldots, z_l\}$ and open sets $V_1, \ldots, V_l$ around $z_1, \ldots, z_l$ respectively along with C^k real valued functions v_i defined on U_i s.t.*

1. $|dv_i| = |dv_j|$ *on* $U_i \cap U_j$

2. $|dv_i| = |Im(z - z_j)^{k_j/2} dz|$ *on* $U_i \cap V_j$.

The kernels $\ker dv_i$ *define a* C^{k-1} *line field on* S *which integrates to give a foliation* $\mathcal{F}$ *on* $S - \{z_1, \ldots, z_l\}$*, with* $k_j + 2$ *pronged singularity at* z_j*. Moreover, given an arc* $\gamma \subset S$*, we have a well-defined measure* $\mu(\gamma)$ *given by* $\mu(\gamma) = |\int_\gamma dv|$ *where* $|dv|$ *is defined by* $|dv|_{U_i} = |dv_i|$.

If each leaf of the measured foliation $(\mathcal{F}, \mu)$ is a finite loop, then $\mathcal{F}$ is called a *finite measured foliation*.

Given a colorable quad-mesh, it is obvious that all the red edges form red loops, each red loop has no self-intersection, two red loops have no intersection either. Similarly, all the blue loops have no intersections. If we subdivide a colorable quad-mesh infinitely many times, all the red loops become infinitely dense and cover all the points on the surface except the singularities in the initial quad-mesh. All the red loops have no intersections, which form a foliation, each red loop is a leaf of the foliation. Similarly, all the blue loops form another foliation. The two foliations transversely intersect each other.

Lemma 2. *Suppose* S *is a closed oriented surface,* Q *is a colorable quadrilateral mesh of the surface, then* Q *induces two finite measured foliations.*

Inversely, if we have two transversal foliations, we can construct a color quad-mesh with minimal number of singularities.

2.4. Strebel Differential

Riemann Surface. Riemann surface theory generalizes the complex analysis to the surface setting. Given a complex function $f : \mathbb{C} \to \mathbb{C}$, $f : x + iy \mapsto u(x, y) + iv(x, y)$, if f satisfies the Cauchy-Riemann equation $u_x = v_y$, $u_y = -v_x$, then f is a *holomorphic function*. If f is invertible, and f^{-1} is also holomorphic, then f is a *bi-holomorphic function*. A two dimensional manifold is called a *surface*. A surface with a complex atlas $\mathcal{A}$, such that all chart transition functions are bi-holomorphic, then it is called a *Riemann surface*, the atlas $\mathcal{A}$ is called a *complex structure*.

Holomorphic Quadratic Differential.

Definition 3 (Holomorphic Quadratic Differentials). *Suppose* S *is a Riemann surface. Let* Φ *be a complex differential form, such that on each local chart with the local complex parameter* $\{z_\alpha\}$*,* $\Phi = \varphi_\alpha(z_\alpha) dz_\alpha^2$*, where* $\varphi_\alpha(z_\alpha)$ *is a holomorphic function.*

A holomorphic quadratic differentials on a genus zero closed surface must be 0. On a genus one closed surface, any holomorphic quadratic differential must be the square of a holomorphic 1-form. According to Riemann-Roch theorem, the dimension of the linear space of all holomorphic quadratic differentials is $3g - 3$ complex dimensional, where the genus $g > 1$.

A point $z_i \in S$ is called a *zero* of Φ, if $\varphi(z_i)$ vanishes. A holomorphic quadratic differential has $4g - 4$ zeros, as shown in Fig. 2. For any point away from zero, we can define a local coordinates $\zeta(p) := \int^p \sqrt{\varphi(z)} dz$, which is the so-called *natural coordinates* induced by Φ. The holomorphic quadratic differential Φ also defines a flat metric on the surface with cone singularities, $d_\Phi := d\zeta d\bar{\zeta}$. The curves with constant real natural coordinates are called the *vertical trajectories*, with constant imaginary natural coordinates *horizontal trajectories*. The trajectories through the zeros are called the *critical trajectories*.

Definition 4 (Strebel[25]). *Given a holomorphic quadratic differential* Φ *on a Riemann surface* S*, if all of its horizontal trajectories are finite, then* Φ *is called a Strebel differential.*

A holomorphic quadratic differential Φ is Strebel, if and only if its critical horizontal trajectories form a finite graph [25].

Measured Foliation vs Holomorphic Quadratic Differentials . Hubbard and Masure proved the following fundamental theorem connecting measured foliation and holomorphic quadratic differentials.

Theorem 1 (Hubbard-Masur [15]). *If* $(\mathcal{F}, \mu)$ *is a measured foliation on a compact Riemann surface* S*, then there is a unique holomorphic quadratic differential* Φ *on* S *whose horizontal foliation is equivalent to* $(\mathcal{F}, \mu)$.

Corollary 1. *Suppose S is a closed compact Riemann surface, $\mathcal{Q}$ is a colorable quadrilateral mesh, then there exists a unique Strebel differential Φ, the horizontal measured foliation of Φ is equivalent to the horizontal foliation induced by $\mathcal{Q}$.*

Similarly, it can be shown there is a unique Strebel differential, whose horizontal foliation is equivalent to the vertical foliation induced by $\mathcal{Q}$.

2.5. Graph-Valued Harmonic Map

Pants Decomposition.

Definition 5 (Admissible Curve System). *On a genus $g > 1$ closed surface S, a set of disjoint, pairwise not homotopic, homotopically nontrivial simple loops $\Gamma = \{\gamma_1, \gamma_2, \cdots, \gamma_n\}$, where $n \leq 3g - 3$ is called an* admissible curve system.

Definition 6 (Pants Decomposition). *On a genus $g > 1$ closed surface S, given an admissible curve system Γ, Γ decomposes the surface into $2g - 2$ pairs of pants $S = \bigcup_{i=1}^{2g-2} P_i$, each pair of pants is a genus 0 surface with 3 boundaries.*

Definition 7 (Pants Decomposition Graph). *Suppose S is a genus $g > 1$ closed surface, Γ is an admissible curve system, which induces a pants decomposition $\{P_i\}$. The corresponding pants decomposition graph $G_\Gamma = (V, E)$ is constructed as follows:*

1. *each node $v_i \in V(G_\Gamma)$ corresponds to a pair of pants P_i;*
2. *each edge $e_k \in E(G_\Gamma)$ corresponds to a loop $\gamma_k\Gamma$, such that e_k connects v_i and v_j if and only if γ_k is shared by P_i and P_j, $\gamma_k = P_i \cap P_j$.*

We assign an edge weight to each edge, the the graph becomes a metric graph.

Definition 8 (Metric Graph). *A graph $G = (V, E)$ is a one dimensional simplicial complex with a vertex set V and an edge set E. A Riemannian metric $\mathbf{d} : E \to \mathbb{R}$ is assigned to each edge $e \in E$. $(G, \mathbf{d})$ is called a metric graph.*

Harmonic Mapping.

Definition 9 (Isothermal Parameters). *Suppose $(S, \mathbf{g})$ is a surface with a Riemannian metric $\mathbf{g}$, the local coordinates (u, v) are called isothermal parameters, if the metric can be represented as $\mathbf{g} = e^{2\lambda(u,v)}(du^2 + dv^2)$, where $\lambda : S \to \mathbb{R}$ is the so-called conformal factor function.*

Chern [6] has proved the existence of isothermal parameters: given any point $p \in S$, there is a neighborhood $U(p) \subset S$ of p, such that isothermal parameters exist on the neighborhood. In the following discussion, isothermal parameters are used by default.

Definition 10 (Harmonic Function). *Given a function defined on a surface with a Riemannian metric, $f : (S, \mathbf{g}) \to \mathbb{R}$, the harmonic energy of the function is defined as $\mathcal{E}(f) := \int_S |\nabla_{\mathbf{g}} f|^2 dA_{\mathbf{g}}$. If f minimizes the harmonic energy, then f is called a harmonic function.*

The local representation of the gradient and the area element under isothermal parameters are as follows: $\nabla_{\mathbf{g}} f(u, v) = \frac{1}{e^{2\lambda(u,v)}}\left(\frac{\partial f(u,v)}{\partial u}, \frac{\partial f(u,v)}{\partial v}\right)^T$, $dA_{\mathbf{g}} = e^{2\lambda(u,v)} du dv$. Suppose $\varphi : (S, \mathbf{g}) \to (G, \mathbf{d})$ is a smooth mapping from a metric surface to a metric graph. The preimage of the vertices of the graph is of zero measure and denoted as Γ. Each edge $e_i \in E$ in the graph is isometrically embedded in $\mathbb{R}$, the preimage of e_i is **topologically a** cylinder C_i. The mapping restricted on C_i is treated as a function, its harmonic energy is well defined by Definition 10. The harmonic energy for the whole map is defined as $\mathcal{E}(\varphi) := \int_{S\setminus\Gamma} |\nabla_{\mathbf{g}} \varphi|^2 dA_{\mathbf{g}}$.

Definition 11 (Graph-valued Harmonic Map). *Suppose $(S, \mathbf{g})$ is a surface with a Riemannian metric $\mathbf{g}$, $(G, \mathbf{d})$ is a metric graph. The mapping $\varphi : (S, \mathbf{g}) \to (G, \mathbf{d})$ is harmonic, if it minimizes the harmonic energy in the homotopy class.*

Gromov and Schoen [9] showed that because the graph $(G, \mathbf{d})$ is with non-positive curvature, the harmonic map exists and is unique in each homotopy class.

Strebel Differential vs. Graph-Valued Harmonic Mapping. Jenkin and Strebel show that if a user prescribes the admissible curve system with the heights, there exists a unique holomorphic quadratic differential with the prescribed combinatorial type and geometry.

Theorem 2 (Jenkin [16] and Strebel [25]). *Given an admissible curve system* $\Gamma = \{\gamma_1, \gamma_2, \cdots, \gamma_n\}$, $n \leq 3g-3$, *and positive numbers (heights)* $\mathbf{h} = \{h_1, h_2, \cdots, h_n\}$, *there exists a unique holomorphic quadratic differential* Φ, *satisfying the following :*

1. *The critical graph of* Φ *partitions the surface into n topological cylinders* $\{C_1, C_2, \cdots, C_n\}$, *such that* γ_k *is the generator of* C_k,
2. *The height of each cylinder* (C_k, d_Φ) *equals to* h_k, $k = 1, 2, \cdots, n$, *where* d_Φ *is the flat metric induced by* Φ.

Wolf [29] showed that the holomorphic quadratic differential Φ can be obtained by the harmonic map from the Riemann surface to the cylindric decomposition graph induced by the curve system Γ with the heights $\mathbf{h}$ as the metric.

Theorem 3 (Wolf[29]). *Given an admissible curve system* Γ, *and an height vector* $\mathbf{h}$, Γ *induces a pants decomposition graph* G_Γ, *with the metric* $\mathbf{h}$. *Let* $\varphi : (S, \mathbf{g}) \to (G_\Gamma, \mathbf{h})$ *be the harmonic map, the Hopf differential* $\Phi = 4\langle \varphi_* \partial_z, \varphi_* \partial_z \rangle_{\mathbf{h}} dz^2$ *is the holomorphic quadratic differential in theorem 2.*

These theorems pave the way to compute the regular quad-meshes.

3. Computational Algorithm

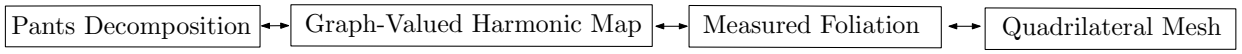

Fig. 3: Algorithmic pipeline.

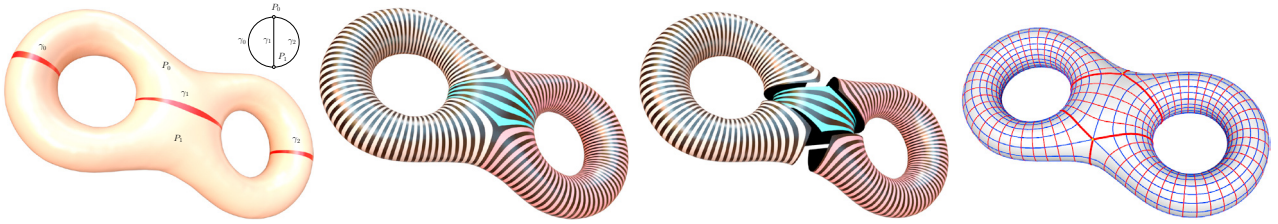

(a) Pants decomposition (b) Foliation (c) Cylindrical decomposition (d) Quadrilateral Mesh

Fig. 4: Foliation generation pipeline.

A surface foliation decomposes the surface into a family of closed loops, such that the decomposition has local tensor product structure. First, we explain the algorithm for a high genus closed surface, then extend it to general cases. Fig. 4 demonstrates the processing pipeline.

3.1. Pants Decomposition

As shown in Fig. 4 frame (a), the first step is *pants decomposition*, which is carried out automatically using the algorithm described in [20]. Given a genus $g > 1$ closed surface S, we automatically compute the g handle loops, then find extra $2g-3$ disjoint simple loops, to form the set of cutting loops, $\{\gamma_1, \gamma_2, \cdots, \gamma_{3g-3}\}$.The cutting loops segment the surface into $2g-2$ pairs of pants, $\{P_1, P_2, \cdots, P_{2g-2}\}$. A pants decomposition can be represented as a graph G, the so-called *pants decomposition graph*, where each pair of pants P_i is represented as a node, and each cutting loop

γ_j is denoted by an edge. Suppose on the surface S, the cutting loop γ_i is shared by two pairs of pants P_j, P_k, then in the graph G, the arc of γ_i connects nodes of P_j and P_k. Furthermore, we associate a positive weight $h_i > 0$ for each edge γ_i in the pants decomposition graph. We use $(G, \mathbf{h})$ to denote the pants decomposition graph G with the weights $\mathbf{h} = (h_1, h_2, \cdots, h_{3g-3})$, and call it the *weighted pants decomposition graph*. The weights can be used to adjust the strip widths.

3.2. Graph-Valued Harmonic Map

As shown in Fig. 4 frame (b), the second step is to compute a foliation based on a harmonic map between the surface and the weighted pants decomposition graph $(G, \mathbf{h})$.

The weighted pants decomposition graph $(G, \mathbf{h})$ can be treated as a *metric space*, where the distance between two points $p, q \in G$ is defined as the length of the shortest path connecting them, and denoted as $d_{\mathbf{h}}(p, q)$.

Given a mapping $f : (S, \mathbf{g}) \to (G, \mathbf{h})$, the pre-image of a node is called a *critical fiber*, and the union of critical fibers is called the *critical graph*, denoted as $\Gamma \subset S$. In general, the critical graph is of 0 measure, then we can define the *harmonic energy* of the mapping f,

$$E(f) := \int_{S \setminus \Gamma} |\nabla_{\mathbf{g}} f|^2 dA_{\mathbf{g}}. \tag{1}$$

If f minimizes the harmonic energy, then f is called a *harmonic map*. Wolf [29] proved the existence and the uniqueness of the harmonic map. The preimage of each non-node point is a closed loop on the original surface. All such closed loops compose a foliation $\mathcal{F}$. The Ribbon graph of the foliation $\mathcal{F}$ is exactly $(G, \mathbf{h})$.

In practice, the surface is approximated by a triangular mesh $M = (V, E, F)$. We use $[v_i, v_j]$ to represent an edge connecting the vertices v_i and v_j. The harmonic energy of a map $f : M \to (G, \mathbf{h})$ is given by

$$E(f) := \frac{1}{2} \sum_{[v_i, v_j]} w_{ij} d_{\mathbf{h}}(f(v_i), f(v_j))^2,$$

where $d_{\mathbf{h}}(\cdot, \cdot)$ is the shortest distance between two points on the graph, w_{ij} is the *cotangent edge weight*. Suppose two faces $[v_i, v_j, v_k]$ and $[v_j, v_i, v_l]$ share the edge $[v_i, v_j]$, then

$$w_{ij} = \cot \theta_k^{ij} + \cot \theta_l^{ji},$$

where θ_k^{ij} represents the corner angle at the vertex v_k in the face $[v_i, v_j, v_k]$.

We use the *non-linear heat flow* method to compute the harmonic map.

1. We homotopically deform γ_i to sweep a cylinder C_i, such that the union of all the cylinders cover the whole surface.
2. Each cylinder C_i is mapped to the edge γ_i, this constructs the initial map f.
3. We diffuse the map to reduce the harmonic energy, until it converges to the harmonic map.

The diffusion process is as follows: at each step, we move the image of each vertex to the *weighted geodesic center* of the images of its neighbors. Suppose after the k-th iteration, we have obtained the mapping $f_k : M \to G$ already, vertices $\{v_j\}$'s are adjacent to the vertex v_i, the weighted geodesic center of $\{f_k(v_j)\}$'s is defined as

$$c_k(v_i) = \text{argmin}_{q \in G} \sum_{j=1}^{n} w_{ij} d_{\mathbf{h}}(f_k(v_j), q)^2.$$

The diffusion process moves the image of v_i to the weighted geodesic center, $f_{k+1}(v_i) \leftarrow c_k(v_i)$. By repeating this procedure, the mapping sequence $\{f_n\}$ converges to the harmonic map.

The harmonic foliation is composed of the fibers, each fiber is a preimage of a point in the graph, $\mathcal{F} = \{f^{-1}(p) | p \in G\}$.

Algorithm 1: Surface Foliation Algorithm for Close Surface.

Input : A close surface $\mathcal{S}$ with genus $g > 1$ and a threshold ε
Output: A foliation $\mathcal{F}$ of $\mathcal{S}$

Construct a pants decomposition of $\mathcal{S}$;
Construct the pants decomposition graph G, assign the edge weight $\mathbf{h}$ to G;
Construct an initial map $f : \mathcal{S} \to G$ by mapping each pair of pants to the corresponding node;
Compute the initial harmonic energy E;
while *true* **do**
  $E_0 \leftarrow E$;
  foreach *vertex* $v_i \in \mathcal{S}$ **do**
    $f(v_i) \leftarrow \mathrm{argmin}_{q \in G} \sum_{j=1}^{n} d_{\mathbf{h}}(f(v_j), q)^2$;
  end
  Calculate the harmonic energy E;
  if $|E - E_0| < \varepsilon$ **then**
    break;
  end
end
foreach $p \in G$ **do**
  Compute the fiber $f^{-1}(p) \in \mathcal{S}$;
end
Return the foliation $\mathcal{F}$ consisting of all fibers;

3.3. Measured Foliations

As shown in Fig. 4 frame (c), the preimages of the nodes form the critical graph Γ, the surface is sliced along Γ and decomposed into $3g - 3$ topological cylinders. Different cylinders are rendered using different colors, all the fibers within one cylinder are homotopic to each other.

For each edge $\gamma_i \in G$, its preimage is a cylinder C_i. The restriction of the harmonic map on the cylinder C_i, $f_i := f|_{C_i}$, can be treated as a harmonic function, $f_i : C_i \to [0, h_i]$. The gradient of f_i can be expressed explicitly. Suppose a face $[v_p, v_q, v_r]$ is in the cylinder C_i, the gradient of the piece-wise linear map f_i on this face is

$$\nabla f_i := \mathbf{n} \times (f_i(v_r)(v_q - v_p) + f_i(v_p)(v_r - v_q) + f_i(v_q)(v_p - v_r))$$

where $\mathbf{n}$ is the normal to the face, by abusing the symbols, v_r represents the position of the vertex v_r. The *Hodge star* operator is defined as ${}^\star\nabla f_i := \mathbf{n} \times \nabla f_i$.

When the mesh triangulation is refined enough, the integration lines of the vector field ${}^\star\nabla f_i$ give the so-called *conjugate foliation* $\mathcal{F}^\star$, that is orthogonal to the original foliation $\mathcal{F}$. We can show that the conjugate foliation $\mathcal{F}^\star$ itself is harmonic as well. The conjugate foliation is depicted in Fig. 4 frame (d), whose fibers are the blue loops.

3.4. Regular Quad-Meshing

Fig. 4 frame (d) illustrates the quadrilateral remeshing step. Basically, given a pair of conjugate foliations $\{\mathcal{F}, \mathcal{F}^\star\}$, we can select some fibers to form a quadrilateral tessellation of the surface.

In more details, each cylinder C_i has two boundaries, $\partial C_i = \tau^+ - \tau^-$. We can find the shortest path γ connecting τ^+ and τ^-. We slice C_i along γ to get a topological quadrilateral, D_i. The integration of a pair of vector fields $({}^\star\nabla f_i, \nabla f_i)$ gives a parameterization $\varphi_i : D_i \to \mathbb{R}^2$, picking a base point $p_0 \in D_i$, $\varphi_i(p) = \int_{p_0}^{p} ({}^\star\nabla f_i, \nabla f_i) dr$, where the integration path $r(t)$ from p_0 to p is arbitrarily chosen within D_i. It can be shown that the parameterization φ_i is angle-preserving, and maps the planar regular grids to the quad-mesh on the surface. The planar horizontal and vertical lines are mapped to red and blue loops on the surface respectively. As shown in Fig. 4, because the parameterization is angle-preserving, the red/blue fibers are orthogonal, and the quadrilateral cells are similar to squares.

3.5. General Cases

Genus One Closed Surface. Fig. 5 shows a pair of conjugate foliations on a genus one closed surface. First, we compute the handle loop γ, set the weight to be the unit, then find a harmonic map from the surface to γ with the unit

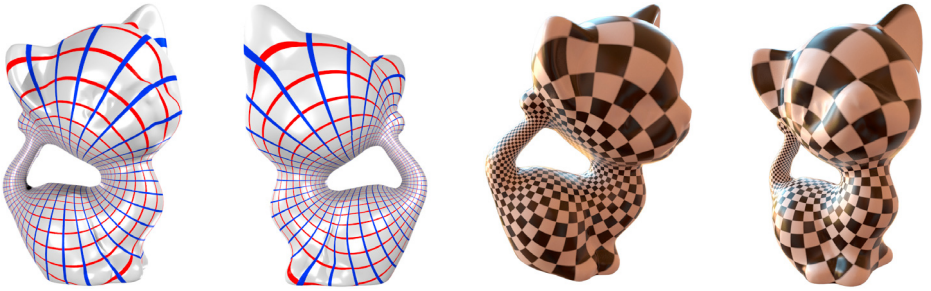

Fig. 5: Conjugate foliations on a genus one surface.

weight, $f : S \to \gamma$. The harmonic map induces a foliation $\mathcal{F}$, whose fibers are the red loops. Locally, f can be treated as a harmonic function. Similarly, we use the Hodge star operator to get the vector field ${}^*\nabla f$, and the integration of ${}^*\nabla$ gives the conjugate harmonic foliation $\mathcal{F}^\star$, whose fibers are the blue loops in the Fig. 5.

Fig. 6: Conjugate foliations on a facial surface.

Topological Disk. As shown in Fig. 6, given a genus zero surface M with a single boundary (a topological disk), we can select four boundary points $\{p_0, p_1, p_2, p_3\}$, which divide the boundary of the surface into four segments, $\{\gamma_0, \gamma_1, \gamma_2, \gamma_3\}$, such that $\partial\gamma_i = p_{i+1} - p_i$.

Then we perform the *double covering* operator: make a copy of M, denoted as $\bar{M}$, reverse the orientation of all faces of $\bar{M}$, then glue M and $\bar{M}$ along the boundary segments γ_0 and γ_2, to form a topological cylinder $\tilde{M}$.

Then we compute a harmonic map from the doubled mesh $\tilde{M}$ to the unit interval, $f : \tilde{M} \to [0, 1]$, such that the boundary loops of $\tilde{M}$ are mapped to the end points of the interval. Then level sets of f gives a foliation $\mathcal{F}$. The integration curves of ${}^\star\nabla f$ gives the conjugate foliation ${}^\star\mathcal{F}$. The restriction of the $\{\mathcal{F}, {}^\star\mathcal{F}\}$ on the original mesh gives the desired pair of conjugate foliations. The harmonic map here can be obtained by solving a sparse linear system.

Fig. 7: Foliations on a genus 0 surface with multiple boundaries.

Open Surfaces with Negative Euler Numbers. Given a surface $M, \chi(M) < 0$, with boundary curves $\partial M = \{\gamma_1, \gamma_2, \cdots, \gamma_n\}$, we first use double covering to obtain a symmetric closed surface $\tilde{M}$. Then we extend $\{\gamma_1, \gamma_2, \cdots, \gamma_n\}$ to a set of cutting loops, generate the pants decomposition, and compute the harmonic map from $\tilde{M}$ to the pants decomposition graph, in turn obtaining a foliation $\mathcal{F}$. By construction, the boundary loops of the original mesh $\{\gamma_i\}$ become the fibers of $\mathcal{F}$. Furthermore, we use the Hodge star operator to obtain the conjugate foliation ${}^*\mathcal{F}$. The restriction of the $\{\mathcal{F}, {}^\star\mathcal{F}\}$ on the original mesh gives the desired pair of conjugate foliations.

Fig. 7 demonstrates the foliation $\mathcal{F}$ on a genus zero surface with multiple boundaries. The original cat model is genus zero surface with 2 boundaries which are the two eyes. To obtain a better foliation, we further puncture through

Model	# of vertices	# of faces	Genus	Boundary	Figure	# of quadrilaterals	Time(ms)
Alex face	80598	160058	0	1	6	289	2274
Kitten	10000	20000	1	0	5	1536	135823
Blood vessel	72312	144620	1	12	8	86840	565012
Eight	3776	7556	2	0	4	7200	32561
Nut	29840	59684	2	0	10	12032	267234
3-hole torus	5996	12000	3	0	9	3840	15142
Deco-cube	7492	15000	5	0	2	14120	10008
Star cup	31029	62062	2	0	11	17408	131114

Table 1: The computation time of foliations of different models.

the bottom of the four feet, the tip of the tail and the two ears, therefore there are 7 more boundary components. In the end, we got a genus zero surface with 9 boundaries.

4. Experimental Results

In this section, we report our experimental results. We have tested our algorithm on synthetic surfaces 9, surfaces scanned from real life 6 and 5, surfaces from mechanical CAD design 10 and reconstructed from medical images 8. Our algorithm is implemented using generic C++, the numerical computation is based on Eigen library [23]. All our experiments are performed on a desktop computer with Intel(R) Core(TM) i7-4770 3.4GHz CPU and 16GB RAM.

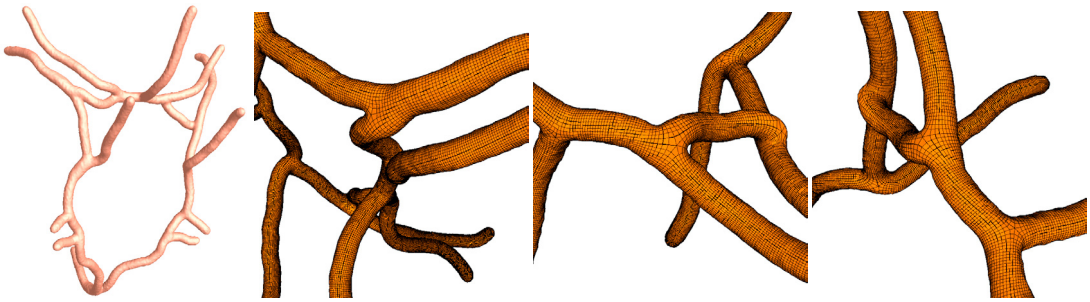

Fig. 8: Quadrilateral mesh for the blood vessel model.

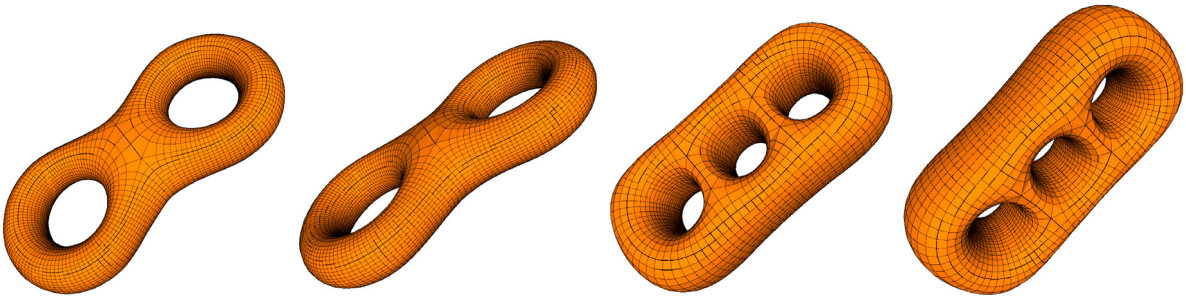

Fig. 9: Quadrilateral meshes for genus two and three models

Topological Generality. As shown in Table 1, in order to test the topological generality of our proposed algorithm, we have process geometric models with various topological types. The scanned human facial surface in Fig. 6 and the cat model Fig. 7 are of genus zero with boundaries; the scanned kitten model Fig. 5 and the blood vessel model Fig. 8 reconstructed from the medical images are of genus one; the eight model Fig. 9 and the mechanical part Fig. 10 are genus 2 surfaces; the three-holed torus Fig. 9 and Decocube model Fig. 2 are with high genus. These results show that our algorithm is general enough to handle surfaces with all topological types.

Efficiency and Stability. We report the running time of our algorithm in this section. The time of computing the foliation are shown in Table 1. The most time-consuming part in the algorithm pipeline is the non-linear heat-diffusion step. From our experiments, we can observe that the computation time is independent of the topology of the surface,

and roughly proportional to the number of vertices except the Alex example which can be solved by using linear system rather than non-linear heat-diffusion. Furthermore, according to the elliptic partial differential equation theory, the solutions smoothly depends on the geometry and the boundary conditions. Namely, the algorithm is stable in terms of geometric noises, insensitive to the triangle mesh qualities.

Quad-Mesh Quality. By examining the figures, especially Fig. 9, Fig. 8, one can observe that the quadrilateral meshes produced by our proposed algorithm have the following merits:

1. Global tensor product structure with the minimal number of singularities;
2. All singularities are with even number valence 6;
3. The foliation leaves except the singularities are of C^∞ smoothness;
4. The whole algorithmic pipeline is fully automatic. It also offers the user the flexibility to choose the optimal one from infinite many choices.

(a) (b) (c) (d)

Fig. 10: Conjugate foliations on a genus 2 mechanical part surface.

On the other hand, our proposed method has the following disadvantages:

1. The sizes of the quadrilateral cells are non-uniform, as shown in the kitten model in Fig. 5 and Fig. 11; Take the starcup model in Fig. 11(c)(d) for example, the quadrilateral cells on the bottom of the starcup are quite huge, and the quadrilateral cells on the handles of the starcup model are very small.
2. The foliation leaves may not align the sharp features, as shown in the mechanical part model in Fig. 10. Some industrial applications may request that the edges of the quadrilateral cells should align the sharp feature of the model. In Fig. 10 (a), the blue curve indicates one sharp feature of the mechanical part surface. (c) shows the vertical foliation on the surface, and we can see the foliation leaves are going through the sharp feature curve rather than aligning it. Eventually the edges of the quadrilateral mesh do not align the sharp feature curve as shown in (d).

5. Conclusions

This work introduces a novel algorithm for quad-mesh generation. It discovers a new category of quad-mesh - generalized regular quad-mesh, which can be applied for surfaces with general topologies and has higher regularity than semi-regular quad-meshes; The generalized regular quad-mesh reduces the number of singularities to the theoretic lower bound; the global tensor product structure is with C^∞ smoothness; the algorithm has solid foliation theory and can be fully automatic.

In the future, we will explore further along foliation mesh generation approach, to find feasible way to improve the uniformity of the cell sizes and the sharp feature alignment.

References

[1] P. Alliez, B. Lévy, A. Sheffer, and N. Ray. Periodic global parameterization. *Acm Transactions on Graphics*, 25(4):1460–1485, 2006.

[2] I. Boier-Martin, H. Rushmeier, and J. Jin. Parameterization of triangle meshes over quadrilateral domains. In *Acm International Conference Proceeding Series*, pages 193–203, 2004.
[3] D. Bommes, B. Lévy, N. Pietroni, E. Puppo, C. Silva, M. Tarini, and D. Zorin. Quad-mesh generation and processing: A survey. *Computer Graphics Forum*, 32(6):51C76, 2013.
[4] N. A. Carr, J. Hoberock, K. Crane, and J. C. Hart. Rectangular multi-chart geometry images. In *Eurographics Symposium on Geometry Processing*, pages 181–190, 2006.
[5] E. Catmull and J. Clark. *Recursively generated B-spline surfaces on arbitrary topological meshes*. ACM, 1998.
[6] S. Chern. An elementary proof of the existence of isothermal parameters on a surface. *Proceedings of the American Mathematical Society*, 6(5):771–782, 1955.
[7] S. Dong, P. T. Bremer, M. Garland, V. Pascucci, and J. C. Hart. Spectral surface quadrangulation. In *ACM SIGGRAPH*, pages 1057–1066, 2006.
[8] H. M. Farkas and I. Kra. *Riemann Surfaces*. Springer, 2004.
[9] M. Gromov and R. Schoen. Harmonic maps into singular spaces and p-adic superrigidity for lattices in groups of rank one. *Publ. Math. IHÉS*, 76:165–246, 1992.
[10] X. Gu, S. Gortler, and H. Hoppe. Geometry images. *ACM Transactions on Graphics (TOG)*, 21(3):355–361, 2002.
[11] X. Gu and S.-T. Yau. *Computational Conformal Geometry*. International Press, 2008.
[12] T. Gurung, D. Laney, P. Lindstrom, and J. Rossignac. Squad: Compact representation for triangle meshes. *Computer Graphics Forum*, 30(2):355C364, 2011.
[13] Y. He, H. Wang, C. W. Fu, and H. Qin. A divide-and-conquer approach for automatic polycube map construction. *Computers & Graphics*, 33(3):369–380, 2009.
[14] J. Huang, M. Zhang, J. Ma, X. Liu, L. Kobbelt, and H. Bao. Spectral quadrangulation with orientation and alignment control. *Acm Transactions on Graphics*, 27(5):1–9, 2008.
[15] J. Hubbard and H. Masur. Quadratic differentials and foliations. *Acta Math.*, (142):221–274, 1979.
[16] J. A. Jenkins. On the existence of certain general extremal metrics. *Ann. of Math.*, 60:440–453, 1957.
[17] F. Kälberer, M. Nieser, and K. Polthier. Quadcover surface parameterization using branched coverings. *Computer Graphics Forum*, 26(3):375–384, 2010.
[18] B. Lévy and Y. Liu. Lp centroidal voronoi tessellation and its applications. *Acm Transactions on Graphics*, 29(4):1–11, 2010.
[19] N. Lei, X. Zheng, J. Jiang, Y.-Y. Lin, and D. X. Gu. Quadrilateral and hexahedral mesh generation based on surface foliation theory. *Computer Methods in Applied Mechanics and Engineering*, 2016.
[20] X. Li, X. Gu, and H. Qin. Surface mapping using consistent pants decomposition. *IEEE Trans. Vis. Comput. Graph.*, 15(4):558–571, 2009.
[21] J. Lin, X. Jin, Z. Fan, and C. C. L. Wang. Automatic polycube-maps. In *International Conference on Advances in Geometric Modeling and Processing*, pages 3–16, 2008.
[22] Y. Liu, W. Xu, J. Wang, L. Zhu, B. Guo, F. Chen, and G. Wang. General planar quadrilateral mesh design using conjugate direction field. In *Siggraph Asia Conference*, pages 1–10, 2011.
[23] T. Marco, P. Nico, C. Paolo, P. Daniele, and P. Enrico. Practical quad mesh simplification. *Computer Graphics Forum*, 29(2):407–418, 2010.
[24] J. F. Remacle, J. Lambrechts, B. Seny, E. Marchandise, A. Johnen, and C. Geuzainet. Blossom-quad: A non-uniform quadrilateral mesh generator using a minimum-cost perfect-matching algorithm. *International Journal for Numerical Methods in Engineering*, 89(9):1102–1119, 2012.
[25] K. Strebel. *Quadratic Differentials*. Springer-Verlag, 1984.
[26] Y. Tong, P. Alliez, D. Cohen-Steiner, and M. Desbrun. Designing quadrangulations with discrete harmonic forms. In *Eurographics Symposium on Geometry Processing, Cagliari, Sardinia, Italy, June*, pages 201–210, 2006.
[27] L. Velho and D. Zorin. *4-8 Subdivision*. Elsevier Science Publishers B. V., 2001.
[28] H. Wang, M. Jin, Y. He, X. Gu, and H. Qin. User-controllable polycube map for manifold spline construction. In *ACM Symposium on Solid and Physical Modeling, Stony Brook, New York, Usa, June*, pages 397–404, 2008.
[29] M. Wolf. On realizing measured foliations via quadratic differentials of harmonic maps to r-trees. *J. D'Analyse Math*, pages 107–120, 1996.
[30] J. Xia, I. Garcia, Y. He, S. Q. Xin, and G. Patow. Editable polycube map for gpu-based subdivision surfaces. In *Symposium on Interactive 3D Graphics and Games*, pages 151–158, 2011.

(a) (b) (c) (d)

Fig. 11: Conjugate foliations on a genus two star-cup model.